Structural and magnetic properties of Pt/Co/Mn-based multilayers

Martin Lonsky,[1,2,*] Myoung-Woo Yoo,[1] Yi-Siou Huang,[1] Jiangchao Qian,[1] Jian-Min Zuo,[1] and Axel Hoffmann[1]
[1]*Materials Research Laboratory and Department of Materials Science and Engineering, University of Illinois at Urbana-Champaign, Urbana, Illinois 61801, USA*
[2]*Institute of Physics, Goethe University Frankfurt, 60438 Frankfurt, Germany*

(Received 18 March 2022; accepted 17 May 2022; published 31 May 2022)

Magnetic multilayers are a rich class of material systems with numerous highly tunable physical parameters that determine both their magnetic and electronic properties. Here, we present a comprehensive experimental study of the system Pt/Co/Mn, which extends the group of Pt/Co/X (X = metal) multilayers that have been investigated thus far. We demonstrate that an increasing Co layer thickness changes the magnetic anisotropy from out of plane to in plane, whereas the deposition of thicker Mn layers leads to a decrease in the saturation magnetization. Temperature-dependent magnetometry measurements reinforce the hypothesis of antiferromagnetic coupling at the Co/Mn interfaces being responsible for the observed Mn thickness dependence of the magnetization reversal. Moreover, magneto-optical imaging experiments indicate systematic changes in magnetic domain patterns as a function of the Co and Mn layer thickness, suggesting the existence of bubblelike domains—potentially even magnetic skyrmions—in the case of sufficiently thick Mn layers, which are expected to contribute to a sizable Dzyaloshinskii-Moriya interaction in the multilayer stacks. We identify Pt/Co/Mn as a highly complex multilayer system with strong potential for further fundamental studies and possible applications.

DOI: 10.1103/PhysRevMaterials.6.054413

I. INTRODUCTION

Metallic magnetic films and multilayers are material systems that offer a high degree of tunability in regard to their magnetic and electronic properties [1–3] and are key to contemporary magnetic applications based on the concepts of spintronics and magnonics [4,5]. The space of controllable parameters includes, but is not limited to, the type of chemical elements, the layer thickness, the number of layer repetitions, and the choice of the deposition method. Especially for magnetic multilayers, there is a wide variety of novel physical phenomena that emerge at the interfaces [6]. One particularly interesting phenomenon in such multilayers is given by the existence of an antisymmetric exchange interaction, the Dzyaloshinskii-Moriya interaction (DMI) [7,8], which under certain conditions may give rise to the presence of magnetic skyrmions even at room temperature [9]. In condensed-matter physics, magnetic skyrmions are topologically distinct chiral spin textures which may find use in future information-processing devices or nonvolatile memory solutions. Such devices may, for instance, be realized by creating, moving, and reading skyrmions in a fast and reliable manner [10–12] or by harnessing the coupled internal eigenmodes of chiral magnetic textures [13–17].

One of the most promising classes of multilayers is given by Pt/Co/X systems, where X corresponds to an additional metallic layer that is required to break spatial inversion symmetry and thus contributes to a significant DMI [18,19]; we note that even in pure Pt/Co multilayer systems a weak DMI has been reported due to the different characters of Pt/Co and Co/Pt interfaces [20]. Pt/Co/X systems are based on scientifically well understood Pt/Co multilayers which have been studied extensively for several decades. Under certain conditions, the addition of a third layer to the Pt/Co-bilayer system may lead to the presence or enhancement of a DMI. In this regard, Ajejas *et al.* recently reported on the dependence of the interfacial DMI strength on the work function difference at the Co/X interface, where they considered various metallic materials X, such as Pd, Ru, and Al [19]. Further works have also focused on several other Pt/Co/X-based multilayers, including Co/Ni/Pt [21], Pt/Co/W [22], Pt/Co/Ta [10], Pt/Co/Ir [23], Pt/Co/Ho [24], and Pt/Co/Cu [25]. In this context, the use of Mn as the third metallic layer X in Pt/Co/X has not been reported thus far, even though the significantly different work functions Φ of Co and Mn, $\Phi_{\mathrm{Co}} = 5.0$ eV and $\Phi_{\mathrm{Mn}} = 4.1$ eV [26], suggest the presence of a considerable interfacial DMI. In addition, further interesting and complex physical phenomena can be expected in Pt/Co/Mn systems due to possible ferro- or antiferromagnetic interlayer and interfacial coupling between Co and Mn, as well as due to the formation of different Mn phases and the occurrence of intermixing at the Co/Mn interface, as reported by various articles on Co/Mn multilayers [27–32]. Despite being well established in the literature, interdiffusion is an often overlooked—but nevertheless important—phenomenon that can occur even in room-temperature-deposited films and typically determines the properties of magnetic heterostructures; see, for example, reports on Co/Gd/Pt [33,34] and Co/Pt [35,36] multilayers.

Motivated by the prospect of rich and complex physical phenomena in a novel metallic heterostructure system, we fabricated polycrystalline $[\mathrm{Pt/Co/Mn}]_n$ multilayer samples

*mlonsky@physik.uni-frankfurt.de

 ©2022 American Physical Society

by means of direct current (dc) magnetron sputtering and carried out a comprehensive characterization of their structural and magnetic properties. In the remainder of this article, we will demonstrate that the magnetic characteristics of Pt/Co/Mn-based multilayers are highly sensitive to the Co and Mn layer thicknesses and can be tuned systematically by careful execution of the deposition processes. Furthermore, systematic changes in the magnetic domain structure as revealed by magneto-optical imaging experiments will be discussed in light of the possible emergence of a DMI and other magnetic interactions.

II. EXPERIMENTAL METHODS

Magnetic Ta(2.0)/[Pt(1.5)/Co(x)/Mn(y)]$_n$/Pt(t_{cap}) multilayers were deposited at room temperature on thermally oxidized Si(100) substrates by means of dc and pulsed dc magnetron sputtering using an AJA International ATC 2200 system. Numbers in parentheses indicate the layer thickness in nanometers. Furthermore, x and y correspond to the thicknesses of the Co and Mn layers, respectively, and the Pt cap layer thickness t_{cap} was chosen to be either 1.5 or 2.0 nm for all samples. The sputtering power was set to 30 W for all materials, and the vacuum chamber was kept at a base pressure better than 2×10^{-8} Torr. During deposition the argon pressure was 3 mTorr. The combination of relatively small power values and a low partial Ar pressure was chosen to increase the deposition time and thereby reduce the error in the thickness of the ultrathin layers. Subsequently, structural characterization was performed by x-ray reflectometry (XRR) on a Bruker D8 Advance system. Modeling and fitting were carried out with the Bruker LEPTOS software package. Scanning transmission electron microscope (STEM) studies of a selected multilayer stack complement the structural analysis of the Pt/Co/Mn heterostructures. To this end, STEM samples were prepared using a focused ion beam (FIB; Thermo Scios2 Dual Beam) microscope lift-out milling technique, and the sample was thinned to ∼50 nm with a careful cleaning processing under 5 and 2 kV. To investigate the elemental configuration, energy dispersive x-ray spectroscopy (EDS) was operated on a STEM (FEI Themis Z Advanced Probe Aberration Corrected Analytical TEM/STEM) at an accelerating voltage of 300 kV (Schottky X-FEG gun) and equipped with four-crystal EDS systems (FEI Super-X) in STEM mode with a semiangle of 18 mrad. All STEM-EDS data were collected for more than 30 min with a 10 μs dwell time and an ∼100 pA probe current. Magnetic properties were measured in a magnetic properties measurement system by Quantum Design, using dc superconducting quantum interference device (SQUID) magnetometry as well as the vibrating sample magnetometer (VSM) option, both yielding consistent results. For samples with a reduced magnetic moment, we have observed the presence of considerable background signals, presumably related to paramagnetic and diamagnetic contributions of the silicon substrate or the sample holder. Therefore, we also recorded hysteresis loops for selected samples using a polar magneto-optical Kerr effect (MOKE) magnetometry setup, for which no spurious signals occurred; see the Supplemental Material for a discussion of these measurements [37]. Furthermore, we utilized a home-built Kerr microscope for magneto-optical imaging of magnetic domain structures in the Pt/Co/Mn samples.

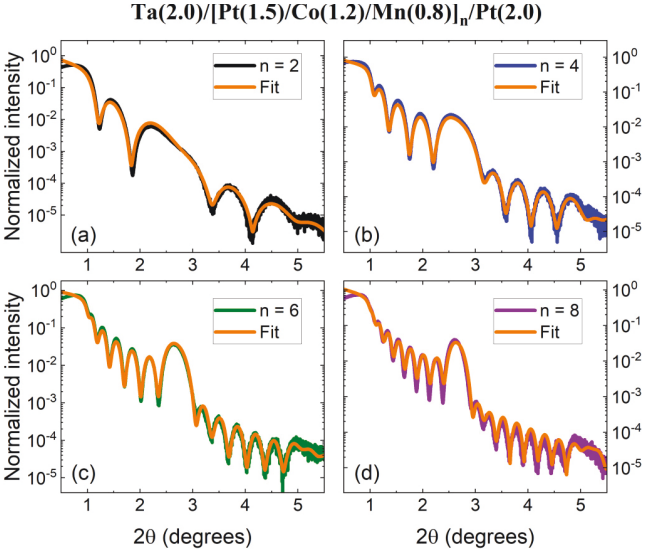

FIG. 1. XRR spectra for samples with varying numbers of repetitions $n = 2, 4, 6, 8$. Depicted are the experimental data as well as fits (orange curves) for angles 2θ (θ is the incident angle) ranging from 0.5° to 5.5°. The maximum interfacial roughness is around 0.4 nm for all samples (see Table I).

III. RESULTS AND DISCUSSION

A. Structural properties

As a first step, we carried out an extensive structural characterization with XRR in order to demonstrate the accuracy and reliability of the magnetron sputtering of [Pt/Co/Mn]$_n$. Figure 1 shows the XRR spectra for angles 2θ between 0.5° and 5.5° for a set of four samples with different numbers n of Pt/Co/Mn trilayer repetitions. Here, θ corresponds to the incident angle of the x-ray beam. Clearly, Kiessig fringes with different wavelengths can be observed for the respective samples. To obtain a better understanding of the data, theoretical XRR spectra are modeled and then fitted to the experimental data by using the LEPTOS software suite. Excellent agreement between the experimental data and the fits (orange curves) can be seen for all four samples. The utilized fit parameters are presented in Table I. Here, t_M corresponds to the layer thickness of material M, and σ_M indicates the layer roughness. It is plausible to assume that the individual Pt, Co, and Mn layer thickness and roughness values are identical for every repetition of the Pt/Co/Mn trilayer. In the bottom row, the nominal thickness values t_M are also presented for the sake of clarity. As can be seen in Table I, the maximum interfacial roughness σ for all multilayer specimens has been determined to be lower than 0.4 nm. This implies that the sputtered films are of good quality. More XRR data for samples with varying Mn and Co layer thicknesses are shown in the Supplemental Material [37].

To gain a deeper understanding of the structural properties in general, we also performed STEM investigations of a selected [Pt/Co/Mn]$_n$ sample with $n = 10$.

TABLE I. Overview of the utilized fit parameters for XRR spectra of Ta(2.0)/[Pt(1.5)/Co(1.2)/Mn(0.8)]$_n$/Pt(2.0) samples with $n = 2, 4, 6, 8$ Pt/Co/Mn trilayer repetitions as displayed in Fig. 1. t_M indicates the layer thickness of material M, and σ_M is the corresponding layer roughness. The bottom row indicates the nominal thickness values t_M.

n	t_{Ta} (nm)	σ_{Ta} (nm)	t_{Pt} (nm)	σ_{Pt} (nm)	t_{Co} (nm)	σ_{Co} (nm)	t_{Mn} (nm)	σ_{Mn} (nm)	$t_{Pt,cap}$ (nm)	$\sigma_{Pt,cap}$ (nm)
2	1.98	0.18	1.46	0.37	1.18	0.20	0.88	0.24	2.00	0.29
4	1.98	0.22	1.50	0.27	1.09	0.29	0.86	0.34	2.12	0.28
6	1.96	0.31	1.54	0.29	1.17	0.21	0.73	0.34	2.19	0.38
8	2.01	0.28	1.61	0.26	1.08	0.20	0.84	0.32	2.28	0.29
Nominal t_M	2.00		1.50		1.20		0.80		2.00	

Figure 2(a) contains a STEM image of a selected Ta(2.0)/[Pt(1.5)/Co(1.2)/Mn(1.2)]$_{10}$/Pt(1.5) sample acquired in the high-angle annular dark-field imaging mode. The multilayer stack is clearly visible and covered with a Pt protection layer deposited during the FIB process in which the STEM sample was prepared. The four pictures in Figs. 2(b)–2(e) correspond to EDS elemental mapping images for the cases of Mn, Co, and Pt and the combination of these chemical elements, respectively. Figure 2(f) illustrates the weight fraction mapping of Mn, Co, and Pt across the multilayer stack. The EDS mapping area and direction (0 to 60 nm) are indicated in Fig. 2(a) by the green box and arrow, respectively. The distance between two adjacent peaks in Fig. 2(f) has been determined to be 4.2 ± 0.3 nm for Pt, while it is 4.3 ± 0.2 nm for both Co and Mn. This is in reasonable agreement with the expected values of 3.9 nm for the given sample. The existence of 10 well-defined maxima for each of the three elements demonstrates that the individual layers are separated and only weak intermixing effects may have occurred at the interfaces. In summary, the XRR and STEM-EDS data verify the precise thickness control in our sputter deposition procedures for Pt/Co/Mn-based multilayers and thereby substantiate the analysis of magnetic properties that is presented hereinafter. In this context, it is important to note that the absence of layer intermixing is crucial for the understanding of the magnetic properties.

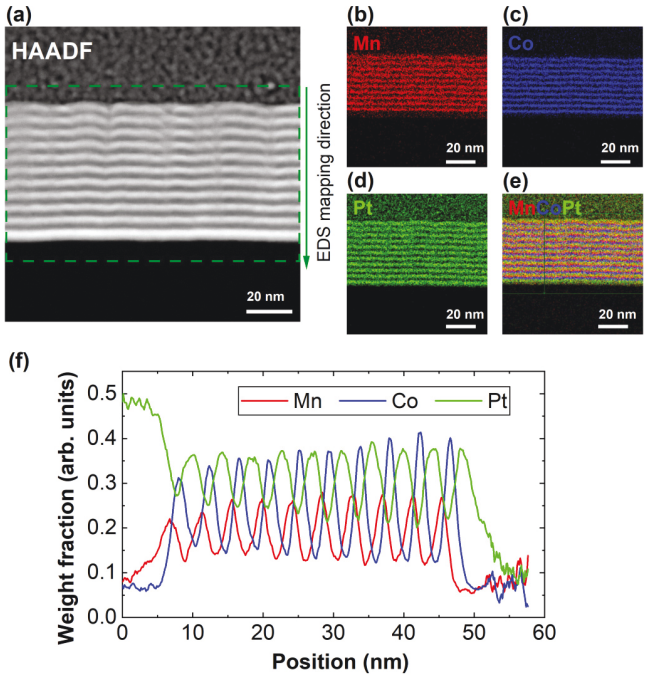

FIG. 2. (a) High-angle annular dark-field imaging (HAADF) scanning transmission electron microscopy (STEM) micrograph of a selected sample, Ta(2.0)/[Pt(1.5)/Co(1.2)/Mn(1.2)]$_{10}$/Pt(1.5). EDS elemental mapping images are shown for (b) Mn, (c) Co, and (d) Pt individually, as well as for (e) all three elements. (f) Weight fraction mapping of Mn, Co, and Pt across the multilayer stack as determined from STEM-EDS measurements. An adjacent averaging filter of 5 pixels is used for smoothing the composition area profiles in (f).

B. Magnetic hysteresis loops at room temperature

As a first step, we have recorded room-temperature magnetic hysteresis curves with SQUID magnetometry measurements. Because of the nontrivial background signal that occurs due to the para- and diamagnetic contributions of the sample holder, possible impurities, and the Si substrate, we also measured hysteresis curves of selected samples by means of a MOKE setup which are in excellent agreement with the SQUID measurements; see the Supplemental Material for a detailed discussion [37].

In the following, we consider samples with different numbers n of Pt/Co/Mn trilayer repetitions. Experiments were performed at 300 K, and the external magnetic field was applied either perpendicular or parallel to the film plane. Figure 3(a) displays hysteresis loops (field perpendicular to film plane) for the four different samples on which the XRR analysis was carried out (see Fig. 1). As is intuitively expected, due

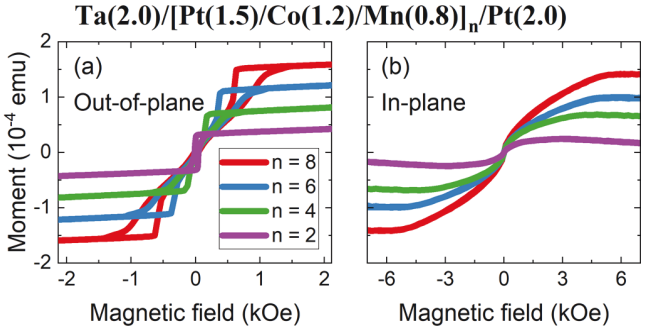

FIG. 3. Magnetic hysteresis loops at room temperature for [Pt/Co/Mn]$_n$ with varying n and the external magnetic field applied (a) out of the film plane and (b) in the film plane. Systematic changes in the hysteresis curves can be explained by modified magnetic energy terms for varying n.

to the higher magnetic (Co) volume, the saturation magnetic moment becomes larger for samples with a higher number of layers. In general, the increasing number of repetitions can lead to modifications in various magnetic energy terms such as the anisotropy or dipolar interaction [38], which explains the observed systematic changes in the hysteresis curves. Furthermore, the sheared nature of out-of-plane (OOP) hysteresis loops is common for systems that exhibit labyrinth domains which may transform into skyrmions (see, for example, Refs. [39,40]). In addition, when comparing the curves to the ones in Fig. 3(b), for which an in-plane magnetic field was applied, it is evident that the samples exhibit a perpendicular magnetic anisotropy. More specifically, the in-plane measurement curves show a much weaker hysteresis than their out-of-plane counterparts. The effective anisotropy values K_{eff} for all aforementioned samples have been determined to lie between 1.2×10^6 and 2.2×10^6 erg/cm^3. In analogy to the work by Wang *et al.* on Pt/Co multilayers, we observe an increasing perpendicular magnetic anisotropy as a function of the number of Pt/Co/Mn trilayer repeats n [38].

Next, we consider the hysteresis loops for samples with varying Mn and Co thicknesses. Hysteresis curves for Ta(2)/[Pt(1.5)/Co(1.2)/Mn(y)]$_2$/Pt(1.5) with varying Mn thickness values y are displayed in Fig. 4(a), where the total magnetic moment divided by the volume of the Co layers is plotted on the ordinate. Most importantly, aside from minor changes in the shape of the hysteresis loops, the saturation magnetization M_s strongly decreases as a function of increasing Mn thickness y. Due to the nontrivial background signal occurring in SQUID measurements of samples with low magnetic moment, we have verified the trend of decreasing M_s with laser-based polar MOKE measurements, which show the Kerr rotation signal is reduced as a function of increasing Mn thickness (not shown). The unusual dependence of the magnetic properties on the Mn layer thickness can be explained by an interfacial exchange coupling between adjacent Co and Mn layers, which may even be accompanied by an antiferromagnetic ordering in the Mn layers in analogy to the findings by Henry and Ounadjela in epitaxial Co/Mn multilayers [29]. Furthermore, the aforementioned work discussed that at the same time an interlayer exchange coupling between adjacent Co layers through the Mn spacer may occur. However, we do not find evidence of the latter scenario due to the lack of an exchange bias effect or changes in the shape of hysteresis loops as a function of the Pt/Co/Mn repetition number n. Apart from this, we cannot rule out slight interdiffusion between the Co and Mn layers, in analogy to the intermixing of Co and Pt reported in Ref. [36], but our STEM measurements lead us to the conclusion that this scenario is rather unlikely. The formation of a Co-Mn alloy at the interface may also lead to the presence of antiferromagnetic coupling within the layers (see, for instance, Ref. [41]). In detail, Men'shikov *et al.* demonstrated that Co-Mn alloys exhibit antiferromagnetism or ferromagnetism or even a mixture of both, depending on the exact composition. Furthermore, at low temperature such alloys may display a behavior similar to a spin glass [41]. We also point out that for low nominal Mn thickness values in some of our samples, there is the possibility that Mn layers were been deposited in a perfectly homogeneous way and instead remained in the island-growth regime, which is common

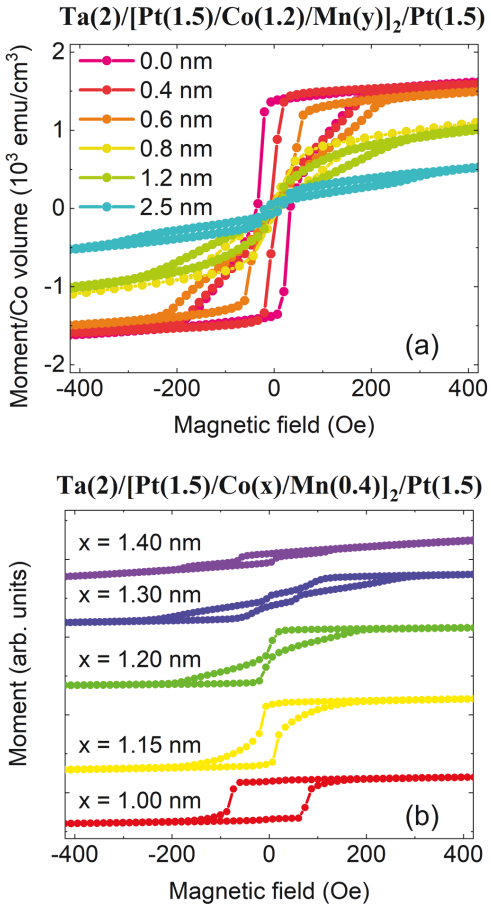

FIG. 4. Magnetic hysteresis curves for [Pt/Co/Mn]$_2$ at 300 K for varying (a) Mn thickness y and (b) Co thickness x. Decreasing M_s for higher y is related to emergent antiferromagnetic coupling within the multilayer stacks. Interfacial anisotropy is strongly dependent on x and therefore explains the change from OOP to IP anisotropy toward higher x.

for sputtered ultrathin films [42] and may affect the magnetic properties. Before a more in-depth investigation of the complex Mn thickness dependence, we now turn to the magnetic properties of Ta(2)/[Pt(1.5)/Co(x)/Mn(0.4)]$_2$/Pt(1.5) with varying Co layer thickness x. The curves in Fig. 4(b) have been shifted with respect to each other for the sake of clarity. Clearly, the magnetization reversal changes from a relatively strong OOP anisotropy behavior toward a more in-plane (IP)-like systematics for increasing Co layer thicknesses, where hysteresis curves become more sheared. This is in good agreement with previous works on Co/Pt multilayers, in which the origin of perpendicular magnetic anisotropy was proven to be interfacial anisotropy, which is highly sensitive to the Co thickness [36,43,44]. Furthermore, a recent work by Denker *et al.* on Ta/CoFeB/MgO films with variable CoFeB thickness yielded comparable results, namely, a transition from OOP to IP anisotropy toward higher thicknesses as indicated by similar hysteresis loops [45].

C. Temperature dependence of magnetic properties

The observed decreasing saturation magnetization for samples with a higher Mn layer thickness served as a

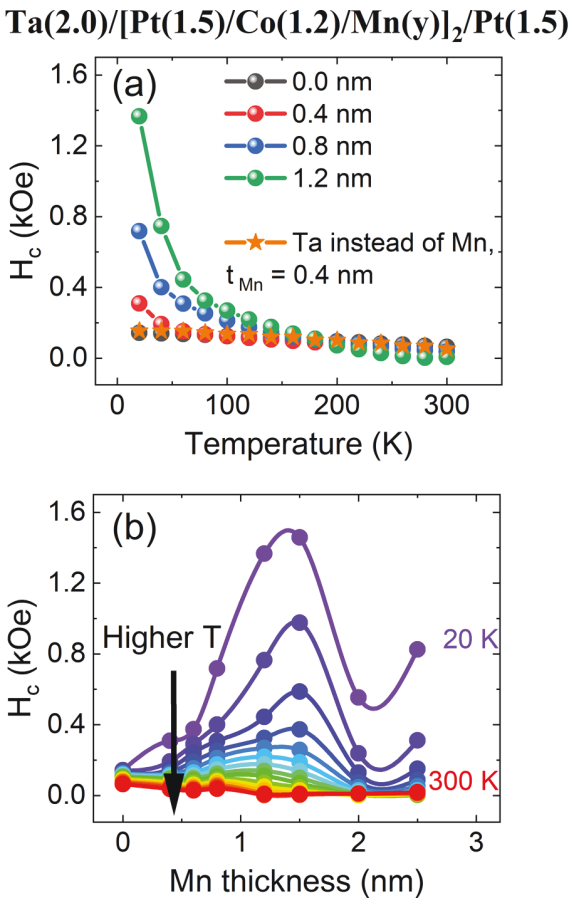

FIG. 5. (a) Temperature-dependent coercive field H_c determined for selected $[Pt/Co/Mn]_2$ samples with varying Mn thickness and a $[Pt/Co/Ta]_2$ reference sample between 20 and 300 K. Toward higher Mn layer thicknesses, H_c increases drastically. (b) H_c plotted against the Mn thickness for different temperatures. A maximum is observed for samples with a Mn thickness of 1.5 nm. Solid lines are a guide to the eye.

motivation for temperature-dependent measurements that could provide further insights into the nature of a possible antiferromagnetic coupling within the multilayer samples. In Fig. 5(a), the coercive field H_c for several $Ta(2)/[Pt(1.5)/Co(1.2)/Mn(y)]_2/Pt(1.5)$ samples with varying Mn thickness y is plotted against temperature between 20 and 300 K. Furthermore, a $[Pt/Co/Ta]_2$ reference sample with 0.4 nm thin layers of Ta instead of Mn has also been investigated. It can be seen that the $[Pt/Co]_2$ and the $[Pt/Co/Ta]_2$ multilayers do not exhibit any significant temperature dependence in H_c. However, a pronounced increase toward low temperatures can be observed for samples containing Mn. In detail, this increase becomes more significant for the case of thicker Mn layers. As shown in Fig. 5(b), there is a maximum for Mn thicknesses between 1.0 and 1.5 nm, whereas the increase in H_c is less pronounced for thickness values outside of this range.

The strong enhancement of the coercive field H_c for samples with intermediate Mn layer thicknesses upon cooling is in good agreement with the hypothesis of an emergent interfacial Co/Mn antiferromagnetic coupling. Our experimental data may also be explained by slight intermixing of Co and Mn and the emergence of a spin-glass-like phase of Co-Mn, in which a higher field (i.e., more energy) is required to rotate the frozen spins into the magnetic field direction. Such a spin-glass-like phase might even be accompanied by antiferromagnetic coupling, which is expected for Co-Mn alloys depending on the exact composition [41]. A pronounced increase in the coercive field toward low temperatures has been reported in a wide range of other materials for various reasons. Selected examples include amorphous Fe-Ni-B metallic glasses [46] and rare-earth-doped permalloy films [47]. While the study by Thomas *et al.* [46] also discusses the existence of a spin-glass-like phase, the increase in coercivity upon cooling for the latter material system is explained by the film structure changing from polycrystalline to amorphous with increasing concentration of dopants. Such a structural transition from polycrystalline to more amorphous films is likewise conceivable for the Co-Mn interfacial region in the studied Pt/Co/Mn samples with varying Mn layer thickness.

Following the discussion of global magnetic properties of Pt/Co/Mn-based multilayers, we will now analyze the spatially resolved magnetic states in these systems.

D. Magneto-optical imaging

Magneto-optical imaging of domains was realized on a home-built Kerr microscope with support from advanced image processing algorithms which include the difference image technique as well as contrast stretching [48]. Due to the decreasing domain size for higher numbers n of Pt/Co/Mn repetitions, we focus on a discussion of measurements for $n = 2$. For samples with higher n, we did not observe any clear signatures of magnetic domains. It should also be emphasized that for samples with Mn layer thicknesses of $y \geqslant 1.0$ nm, the Kerr signal becomes increasingly weaker, and thus, magneto-optical imaging with adequate resolution is not possible with our current setup. Figure 6(a) shows representative images of samples with varying Mn thickness y at zero external magnetic field after saturation with an out-of-plane field. We observe a dendritic domain structure at the lowest Mn thickness $y = 0.4$ nm. The average size of the magnetic domains is clearly lower for the case of $y = 0.6$ nm. For an even higher Mn thickness of $y = 0.8$ nm, we mostly observe bubblelike domains, which could potentially be magnetic skyrmions that are formed as a consequence of the DMI introduced by the Mn layer. However, despite the expected presence of interfacial DMI due to the difference in Co and Mn work functions [19], the available experimental data is solely a hint and not unambiguous proof of the bubblelike objects being skyrmions. A more detailed investigation of the static and dynamic properties of these bubblelike domains is beyond the scope of the present work.

In Fig. 6(b), three further representative images are shown for samples with varying Co thickness x at zero external field after saturation. Here, the size of the domains likewise changes systematically as a function of the Co layer thickness, which is in concordance with MOKE studies of CoFeB films with varying thickness [45]. Despite the rather small variations of the Co layer thickness, the MOKE images in Fig. 6(b) display significant changes in the domain pattern.

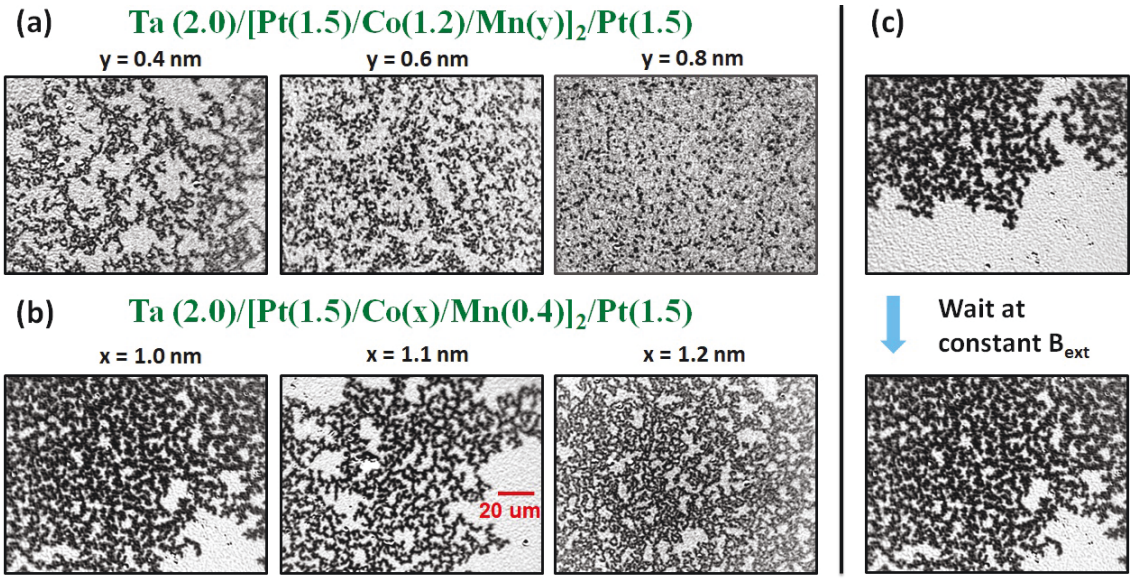

FIG. 6. MOKE images of $[Pt/Co/Mn]_2$ multilayers for selected samples with varying (a) Mn layer and (b) Co layer thickness. The scale bar (red) corresponds to a length of 20 μm. A sufficiently thick Mn layer leads to the presence of bubble domains or, potentially, skyrmions. (c) Example of domain structure changes within a time interval of $T = 10$ s at a constant external field $B_{ext} \approx 20$ Oe for a $Ta(2)/[Pt(1.5)/Co(1)/Mn(0.4)]_2/Pt(1.5)$ specimen.

Finally, Fig. 6(c) displays the interesting observation that the domain state changes as a function of time even at a constant magnetic field. This is attributed to the pinning and depinning of domain walls at defects which represent local minima in the complex energy landscape. Both MOKE images of the sample $Ta(2)/[Pt(1.5)/Co(1)/Mn(0.4)]_2/Pt(1.5)$ are taken at an external magnetic field of approximately 20 Oe applied perpendicular to the film plane. The top image was taken right after the field value was reached, whereas the bottom image was acquired after a waiting time of 10 s at a constant field value. Our observations are in good agreement with Pt/Co multilayers studied by Woodward *et al.* which display a similar behavior [49]. A more detailed discussion of this magnetic relaxation effect be found in the Supplemental Material [37].

IV. SUMMARY AND CONCLUSION

In this work, we have experimentally characterized a Pt/Co-based multilayer system, namely, $[Pt/Co/Mn]_n$. Structural investigations via XRR and STEM provided clear evidence of the high quality of the sputtered layers and also demonstrated the accuracy as well as reliability of the deposition process. Magnetic characterization by means of polar Kerr microscopy and SQUID/VSM magnetometry revealed a systematic and complex behavior of this material system. While the magnetic anisotropy can be tuned from out of plane to in plane by increasing the Co layer thickness, a sufficiently thick Mn layer leads to the emergence of bubblelike magnetic domains—potentially even skyrmions—as well as to a reduction in the total magnetic moment. The latter is ascribed to the emergence of interfacial Co/Mn antiferromagnetic coupling. Furthermore, a Co-Mn alloy possibly forms in a narrow interfacial region and may contain antiferromagnetic regions, which in the corresponding samples contribute to a strong increase in the coercive field at low temperatures. This behavior is most pronounced for Mn thicknesses around 1.5 nm and becomes less relevant for both higher and lower thickness values. Finally, we also observed a universal, time-dependent dendriticlike growth of magnetic domains in the Pt/Co/Mn material system.

We suggest the investigation of this material system by means of Lorentz transmission electron microscopy or other comparable advanced imaging methods in order to reveal the character of the bubblelike domains unequivocally. In addition, such advanced imaging methods will allow for a more detailed characterization of multilayers with a high number of Pt/Co/Mn repetitions, where the average domain size is significantly smaller than that for $n = 2$ and therefore cannot be studied with our Kerr microscope. Alternatively, studying the current-driven dynamics of the observed bubblelike objects will also help us to understand whether they are skyrmions or not.

In conclusion, it was shown that tuning and understanding the magnetic properties of $[Pt/Co/Mn]_n$ require careful engineering of and control over the structural properties of the individual metallic layers. While our STEM measurements do not indicate considerable intermixing of Co and Mn, it will be interesting to explore how even weak Co-Mn intermixing could be controlled more precisely, for instance, by varying deposition parameters systematically and by inserting ultrathin Cu diffusion barriers, as has been done for the case of $[Co/Pt]_n$ multilayers [36,50], or by exploiting atomically thin two-dimensional materials such as graphene [51,52].

ACKNOWLEDGMENTS

The authors would like to thank F. Ajejas for fruitful discussions on magnetic multilayers and D. Vaz for instructive comments on intermixing effects and diffusion barriers. Support during the sputtering process provided by

J. Gibbons and S. Siddiqui is also gratefully acknowledged. M.L. acknowledges the financial support from the German Science Foundation (Deutsche Forschungsgemeinschaft, DFG) through Research Fellowship No. LO 2584/1-1. The sample fabrication, structural and magnetic characterization, and data analysis and manuscript preparation were supported by the NSF through the University of Illinois at Urbana-Champaign Materials Research Science and Engineering Center (Grant No. DMR-1720633) and were carried out in part in the Materials Research Laboratory Central Research Facilities, University of Illinois. The transmission electron microscopy measurements were supported by the US Department of Energy, Office of Science, Materials Science and Engineering Division, under Contract No. DE-SC0022060.

[1] I. K. Schuller, S. Kim, and C. Leighton, Magnetic superlattices and multilayers, J. Magn. Magn. Mater. **200**, 571 (1999).

[2] L. H. Bennett and R. E. Watson, *Magnetic Multilayers* (World Scientific, Singapore, 1994).

[3] R. E. Camley and R. L. Stamps, Magnetic multilayers: Spin configurations, excitations and giant magnetoresistance, J. Phys.: Condens. Matter **5**, 3727 (1993).

[4] E. Y. Vedmedenko, R. K. Kawakami, D. D. Sheka, P. Gambardella, A. Kirilyuk, A. Hirohata, C. Binek, O. Chubykalo-Fesenko, S. Sanvito, B. J. Kirby, J. Grollier, K. Everschor-Sitte, T. Kampfrath, C.-Y. You, and A. Berger, The 2020 magnetism roadmap, J. Phys. D **53**, 453001 (2020).

[5] C. Back, V. Cros, H. Ebert, K. Everschor-Sitte, A. Fert, M. Garst, T. Ma, S. Mankovsky, T. L. Monchesky, M. Mostovoy, N. Nagaosa, S. S. P. Parkin, C. Pfleiderer, N. Reyren, A. Rosch, Y. Taguchi, Y. Tokura, K. von Bergmann, and J. Zang, The 2020 skyrmionics roadmap, J. Phys. D **53**, 363001 (2020).

[6] F. Hellman *et al.*, Interface-induced phenomena in magnetism, Rev. Mod. Phys. **89**, 025006 (2017).

[7] I. Dzyaloshinsky, A thermodynamic theory of "weak" ferromagnetism of antiferromagnetics, J. Phys. Chem. Solids **4**, 241 (1958).

[8] T. Moriya, Anisotropic superexchange interaction and weak ferromagnetism, Phys. Rev. **120**, 91 (1960).

[9] W. Jiang, G. Chen, K. Liu, J. Zang, S. G. te Velthuis, and A. Hoffmann, Skyrmions in magnetic multilayers, Phys. Rep. **704**, 1 (2017).

[10] S. Woo, K. Litzius, B. Krüger, M.-Y. Im, L. Caretta, K. Richter, M. Mann, A. Krone, R. M. Reeve, M. Weigand, P. Agrawal, I. Lemesh, M.-A. Mawass, P. Fischer, M. Kläui, and G. S. D. Beach, Observation of room-temperature magnetic skyrmions and their current-driven dynamics in ultrathin metallic ferromagnets, Nat. Mater. **15**, 501 (2016).

[11] S. Woo, K. M. Song, X. Zhang, M. Ezawa, Y. Zhou, X. Liu, M. Weigand, S. Finizio, J. Raabe, M.-C. Park, K.-Y. Lee, J. W. Choi, B.-C. Min, H. C. Koo, and J. Chang, Deterministic creation and deletion of a single magnetic skyrmion observed by direct time-resolved x-ray microscopy, Nat. Electron. **1**, 288 (2018).

[12] K. Everschor-Sitte, J. Masell, R. M. Reeve, and M. Kläui, Perspective: Magnetic skyrmions—Overview of recent progress in an active research field, J. Appl. Phys. **124**, 240901 (2018).

[13] J. Kim, J. Yang, Y.-J. Cho, B. Kim, and S.-K. Kim, Coupled gyration modes in one-dimensional skyrmion arrays in thin-film nanostrips as new type of information carrier, Sci. Rep. **7**, 45185 (2017).

[14] J. Kim, J. Yang, Y.-J. Cho, B. Kim, and S.-K. Kim, Coupled breathing modes in one-dimensional skyrmion lattices, J. Appl. Phys. **123**, 053903 (2018).

[15] M. Lonsky and A. Hoffmann, Dynamic excitations of chiral magnetic textures, APL Mater. **8**, 100903 (2020).

[16] M. Lonsky and A. Hoffmann, Coupled skyrmion breathing modes in synthetic ferri- and antiferromagnets, Phys. Rev. B **102**, 104403 (2020).

[17] Z. Chen and F. Ma, Skyrmion based magnonic crystals, J. Appl. Phys. **130**, 090901 (2021).

[18] H. Jia, B. Zimmermann, M. Hoffmann, M. Sallermann, G. Bihlmayer, and S. Blügel, Material systems for FM-/AFM-coupled skyrmions in Co/Pt-based multilayers, Phys. Rev. Materials **4**, 094407 (2020).

[19] F. Ajejas, Y. Sassi, W. Legrand, S. Collin, A. Thiaville, J. P. Garcia, S. Pizzini, N. Reyren, V. Cros, and A. Fert, Element-selective modulation of interfacial Dzyaloshinskii-Moriya interaction in Pt|Co|metal based multilayers, arXiv:2109.00761.

[20] A. W. J. Wells, P. M. Shepley, C. H. Marrows, and T. A. Moore, Effect of interfacial intermixing on the Dzyaloshinskii-Moriya interaction in Pt/Co/Pt, Phys. Rev. B **95**, 054428 (2017).

[21] J. A. Brock, S. A. Montoya, M.-Y. Im, and E. E. Fullerton, Energy-efficient generation of skyrmion phases in Co/Ni/Pt-based multilayers using Joule heating, Phys. Rev. Materials **4**, 104409 (2020).

[22] W. Jiang, S. Zhang, X. Wang, C. Phatak, Q. Wang, W. Zhang, M. B. Jungfleisch, J. E. Pearson, Y. Liu, J. Zang, X. Cheng, A. Petford-Long, A. Hoffmann, and S. G. E. te Velthuis, Quantifying chiral exchange interaction for Néel-type skyrmions via Lorentz transmission electron microscopy, Phys. Rev. B **99**, 104402 (2019).

[23] D. Khadka, S. Karayev, and S. X. Huang, Dzyaloshinskii–Moriya interaction in Pt/Co/Ir and Pt/Co/Ru multilayer films, J. Appl. Phys. **123**, 123905 (2018).

[24] L. Liu, X. Zhao, W. Liu, Y. Song, X. Zhao, and Z. Zhang, Influence of rare earth metal Ho on the interfacial Dzyaloshinskii–Moriya interaction and spin torque efficiency in Pt/Co/Ho multilayers, Nanoscale **12**, 12444 (2020).

[25] S. Schlotter, P. Agrawal, and G. S. D. Beach, Temperature dependence of the Dzyaloshinskii-Moriya interaction in Pt/Co/Cu thin film heterostructures, Appl. Phys. Lett. **113**, 092402 (2018).

[26] H. B. Michaelson, The work function of the elements and its periodicity, J. Appl. Phys. **48**, 4729 (1977).

[27] T. Kai, Interlayer exchange coupling and electronic structure of Co/Mn multilayers, J. Magn. Magn. Mater. **214**, 167 (2000).

[28] B. Zhang, C.-B. Wu, and W. Kuch, Tailoring interlayer coupling and coercivity in Co/Mn/Co trilayers by controlling the interface roughness, J. Appl. Phys. **115**, 233915 (2014).

[29] Y. Henry and K. Ounadjela, Evidence for a Direct *d*-*d* Hybridization Mechanism for the Interlayer Exchange Coupling in Epitaxial Co/Mn Multilayers, Phys. Rev. Lett. **76**, 1944 (1996).

[30] I. Ishida and A. Sagawa, Mechanisms of coercive force in Co/Mn multilayers, J. Magn. Magn. Mater. **279**, 261 (2004).

[31] K. Uchiyama, I. Ishida, K. Hamada, E. Hirota, A. Okada, and T. Hayashi, Saturation magnetic moments of Co/Mn multilayers, J. Magn. Magn. Mater. **156**, 429 (1996).

[32] I. Ishida and S. Morita, Enhanced magnetic moments in Co/Mn multilayers: Structural and magnetic investigations, J. Magn. Magn. Mater. **267**, 204 (2003).

[33] T. Nishimura, D.-Y. Kim, D.-H. Kim, Y.-S. Nam, Y.-K. Park, N.-H. Kim, Y. Shiota, C.-Y. You, B.-C. Min, S.-B. Choe, and T. Ono, Interfacial Dzyaloshinskii-Moriya interaction and dampinglike spin-orbit torque in [Co/Gd/Pt]N magnetic multilayers, Phys. Rev. B **103**, 104409 (2021).

[34] T. Nishimura, M. Haruta, D.-H. Kim, Y. Shiota, H. Iwaki, D. Kan, T. Moriyama, H. Kurata, and T. Ono, Fabrication of Ferrimagnetic Co/Gd/Pt Multilayers with Structural Inversion Symmetry Breaking, J. Magn. Soc. Jpn. **44**, 9 (2020).

[35] C.-H. Su, S.-C. Lo, J. van Lierop, K.-W. Lin, and H. Ouyang, The intermixing induced perpendicular magnetic anisotropy in ultrathin Co/Pt multilayers, J. Appl. Phys. **105**, 07C316 (2009).

[36] S. Bandiera, R. C. Sousa, B. Rodmacq, and B. Dieny, Enhancement of perpendicular magnetic anisotropy through reduction of Co-Pt interdiffusion in (Co/Pt) multilayers, Appl. Phys. Lett. **100**, 142410 (2012).

[37] See Supplemental Material at http://link.aps.org/supplemental/10.1103/PhysRevMaterials.6.054413 for additional experimental data and a more detailed discussion of magnetometry and x-ray reflectometry measurements.

[38] X. Wang, Y. Wei, K. He, Y. Liu, Y. Huang, Q. Liu, J. Wang, and G. Han, Effect of the repeat number and Co layer thickness on the magnetization reversal process in $[Pt/Co(x)]_N$ multilayers, J. Phys. D **53**, 215001 (2020).

[39] T. Lin, H. Liu, S. Poellath, Y. Zhang, B. Ji, N. Lei, J. J. Yun, L. Xi, D. Z. Yang, T. Xing, Z. L. Wang, L. Sun, Y. Z. Wu, L. F. Yin, W. B. Wang, J. Shen, J. Zweck, C. H. Back, Y. G. Zhang, and W. S. Zhao, Observation of room-temperature magnetic skyrmions in Pt/Co/W structures with a large spin-orbit coupling, Phys. Rev. B **98**, 174425 (2018).

[40] A. Soumyanarayanan, M. Raju, A. L. G. Oyarce, A. K. C. Tan, M.-Y. Im, A. P. Petrović, P. Ho, K. H. Khoo, M. Tran, C. K. Gan, F. Ernult, and C. Panagopoulos, Tunable room-temperature magnetic skyrmions in Ir/Fe/Co/Pt multilayers, Nat. Mater. **16**, 898 (2017).

[41] A. Z. Men'shikov, G. Takzei, Y. A. Dorofeev, V. A. Kazantsev, A. K. Kostyshin, and I. I. Sych, The magnetic phase diagram of cobalt-manganese alloys, Zh. Eksp. Teor. Fiz. **89**, 1269 (1985).

[42] H. J. Waring, N. A. B. Johansson, I. J. Vera-Marun, and T. Thomson, Zero-Field Optic Mode Beyond 20 GHz in a Synthetic Antiferromagnet, Phys. Rev. Applied **13**, 034035 (2020).

[43] P. F. Carcia, Perpendicular magnetic anisotropy in Pd/Co and Pt/Co thin-film layered structures, J. Appl. Phys. **63**, 5066 (1988).

[44] W. B. Zeper, F. J. A. M. Greidanus, P. F. Carcia, and C. R. Fincher, Perpendicular magnetic anisotropy and magneto-optical Kerr effect of vapor-deposited Co/Pt-layered structures, J. Appl. Phys. **65**, 4971 (1989).

[45] C. Denker, S. Nielsen, E. Lage, M. Römer-Stumm, H. Heyen, Y. Junk, J. Walowski, K. Waldorf, M. Münzenberg, and J. McCord, Observation of multi-skyrmion objects created by size and density control in Ta/CoFeB/MgO films, arXiv:2011.07336.

[46] S. Thomas, G. Pookat, S. S. Nair, M. Daniel, B. Dymerska, A. Liebig, S. H. Al-Harthi, R. V. Ramanujan, M. R. Anantharaman, J. Fidler, and M. Albrecht, Exchange bias effect in partially oxidized amorphous Fe–Ni–B based metallic glass nanostructures, J. Phys.: Condens. Matter **24**, 256004 (2012).

[47] C. Luo, Y. Fu, D. Zhang, S. Yuan, Y. Zhai, S. Dong, and H. Zhai, Temperature dependent coercivity and magnetization of light rare-earth Nd doped permalloy thin films, J. Magn. Magn. Mater. **374**, 711 (2015).

[48] R. Schäfer, Investigation of domains and dynamics of domain walls by the magneto-optical Kerr-effect, in *Handbook of Magnetism and Advanced Magnetic Materials* (Wiley, Chichester, UK, 2007).

[49] R. C. Woodward, A. M. Lance, R. Street, and R. L. Stamps, Variation of the magnetic domain structure with reversal field (invited), J. Appl. Phys. **93**, 6567 (2003).

[50] S. Bandiera, R. C. Sousa, B. Rodmacq, L. Lechevallier, and B. Dieny, Effect of a Cu spacer between Co and Pt layers on the structural and magnetic properties in $(Co/Cu/Pt)_5/Pt$ type multilayers, J. Phys. D **46**, 485003 (2013).

[51] W. K. Morrow, S. J. Pearton, and F. Ren, Review of graphene as a solid state diffusion barrier, Small **12**, 120 (2016).

[52] J. Hong, S. Lee, S. Lee, H. Han, C. Mahata, H.-W. Yeon, B. Koo, S.-I. Kim, T. Nam, K. Byun, B.-W. Min, Y.-W. Kim, H. Kim, Y.-C. Joo, and T. Lee, Graphene as an atomically thin barrier to Cu diffusion into Si, Nanoscale **6**, 7503 (2014).